

A Study on Large Eddy Simulation of High Reynolds Number Flow Past A Square Cylinder

Samiran Sandilya, Amit Kumar

Mechanical Engineering Department, RGPV/Bhopal Institute of Technology and Science, Bhopal, Madhya Pradesh India

ABSTRACT

Flow past a square cylinder has been studied extensively for over a century, because of its interesting flow features and practical applications. This problem is of fundamental interest as well as important in many engineering applications. The characteristics of flow around a square cylinder placed at symmetric condition are governed by the Reynolds number (Re). In the present study two dimensional simulations of flow past a square cylinder have been carried out for a Reynolds number of 21400. It has been studied numerically using the large-eddy simulation technique. The modeling of the problem is done by ANSYS 17.1 preprocessing software.

Keywords : Square Cylinder, Reynolds Number, Modeling, Large Eddy Simulation

I. INTRODUCTION

The phenomenon of flow separation and bluff body wakes has long been intensively studied because of its fundamental significance in flow physics and its practical importance in aerodynamic and hydrodynamic applications. The flow of fluid past cylinders of various cross sections represents an idealization of several industrially important applications. It is readily acknowledged that a systematic study of the flow past a single cylinder not only provides valuable insights into the nature of flow, but also serves as a useful starting point to understand the flow in real-life multi-cylinder and other applications such as flow past pipelines near the ground, flow past building construction, suspension bridge, heat transfer enhancement in heat exchangers and forced-air cooling of board-mounted electronic components etc.

The presence of the fluid viscosity slows down the fluid particles very close to the solid surface and forms a thin slow-moving fluid layer called a boundary layer. The flow velocity is zero at the surface to satisfy the no-slip boundary condition. Inside the boundary layer, flow momentum is quite low since it experiences a strong viscous flow resistance. Therefore, the boundary layer flow is sensitive to the external pressure gradient. If the pressure decreases in the direction of the flow, the pressure gradient is said to be favorable. In this case, the pressure force can assist the fluid movement and there is no flow retardation. However, if the pressure is increasing in the direction of the flow, an adverse pressure gradient condition exists. In addition to the When a fluid particle flows within the boundary layer around the circular cylinder, it has been observed experimentally that, the pressure is maximum at the stagnation point and gradually decreases along the front half of the cylinder. The flow stays attached in this favorable pressure region as

expected. However, the pressure starts to increase in the rear half of the cylinder and at this time particle experiences an adverse pressure gradient. Consequently, the flow separates from the surface, creating a highly turbulent region behind the cylinder called the wake. The pressure inside the wake region remains low as the flow separates and a net pressure force (pressure drag) is produced.

II. LITERATURE SURVEY

Mohammad Saeedi et al.[1][2016] Large eddy simulation of planar shear flow past a square cylinder has been investigated. Dynamic Smagorinsky model has been used to model sub grid scale stress. The shear parameter, K , namely the non dimensional stream wise velocity gradient in the lateral direction, is 0.0, 0.1 and 0.2. Reynolds number based on the centerline velocity is fixed at $Re=22000$. The time and span-averaged velocity components, pressure coefficient, Reynolds stresses for uniform are in good agreement with the literature. In shear flow the calculated flow structure and mean velocity components are shown to be markedly different from those of the uniform flow. With increasing shear parameter, the cylinder wake is dominated by clockwise vortices. Both the velocity components in shear flow are compared with respective components in uniform flow. Comparison of normal and shear stresses between shear and no shear case have also been presented.

Rusdin [2][2017] Two-dimensional Reynolds Averaged Navier Stokes (RANS) turbulence model simulations for a flow past a square block with $Re = 22000$ are presented in this paper. An available modified $k-\varepsilon$ turbulence model, which is an improved version of the standard $k-\varepsilon$ turbulence model, is applied to simulate experiment cases of vortex shedding around a square block. The performance evaluation of the modified model is conducted by assessing its results with the results of the standard $k-\varepsilon$ turbulence model based on the similarity with the experiment measurement data. It

is found that the modified model improves the drag coefficient by about 16%, the Strouhal number by about 1.5%, and the length recirculation zone by about factor two compared to that of the standard model. The RMSE values indicate a significant improvement of the time averaged velocity along the centre line by about 59% and the velocity profile above the square block by about 6% when the modified model is applied. Generally, the modified $k-\varepsilon$ model indicates advantages compared with the standard $k-\varepsilon$ model. However, discrepancy is found between the model result and the experiment observation for the free stream velocity at downstream and it may be necessary to consider the 3D effect on turbulent fluctuation in further studies.

Xiaowang Sun [3][2015] This paper presents large eddy simulation (LES) results of convective heat transfer and incompressible-fluid flow around a square cylinder (SC) at Reynolds numbers in the range from 103 to 3.5 ,105. The LES uses the swirling-strength based sub-grid scale (SbSGS) model. Several flow properties at turbulent regime are explored, including lift and drag coefficients, time-spanwise averaged sub-grid viscosity, and Kolmogorov micro-scale. Local and mean Nusselt numbers of convective heat transfer from the SC under isothermal wall temperature are predicted and compared with empirical results.

Prasenjit Dey [4][2015] The numerical analysis is carried out at low Reynolds number, $Re \frac{1}{4} 100 \& 180$ for different nondimensional thorn lengths ($l' \frac{1}{4} 0.2, 0.4 \& 0.6$), different inclination angles ($q \frac{1}{4} 5_, 10_, 15_ \text{ and } 20_$) and two different thorn positions. It is found that drag and lift reduction can be achieved by attaching the thorn on a square cylinder. It is observed that the fluctuation of the drag force as well as the lift force is reduced and there is a comparatively large variation of drag and lift when the thorn is placed at the front stagnation point instead of placing at rear stagnation point. The reduction of drag and lift coefficient are directly

proportional to thorn length and thorn inclination angle. It is found that the drag and lift are minimized by 16% & 46% for $Re \frac{1}{4} 100$ respectively, and 22% & 60% for $Re \frac{1}{4} 180$ compared to a square model (without thorn)

Mohammad Saeedi[5][2015] In this paper, large-eddy simulation (LES) has been performed to investigate the turbulent wake behind a wall-mounted square cylinder. The flow features a relatively high cylinder aspect ratio of 4, a Reynolds number of 12,000 (based on the free-stream velocity and cylinder side length), and a thin developing boundary layer with a thickness of only 18 % of the obstacle height. These characteristics of the flow impose challenges to LES for accurate simulation of large energetic eddies induced by the cylinder and their intense interactions with the thin developing boundary layer. The coherent flow structures around the cylinder have been studied based on the instantaneous and time-averaged resolved velocity and pressure fields. The local kinetic energy transfer between the resolved and subgrid scales and the streamwise evolution of the subgrid-scale viscosity have been investigated to provide physical insights into the subgrid-scale dynamics. The LES predictions of the flow statistics have been validated against a set of recently reported wind-tunnel experimental data.

Mingyue Liu et al.,[6] [2015] The Deep Draft Semi-Submersible (DDS) concepts are known for their favorable vertical motion performance. However, the DDS may experience critical Vortex-Induced Motion (VIM) stemming from the fluctuating forces on the columns. In order to investigate the current-induced excitation forces of VIM, an experimental study of flow characteristics around four square-section cylinders in a square configuration is presented. A number of column spacing ratios and array attack angles were considered to investigate the parametric influences. The results comprise flow patterns, drag and lift forces, as well as Strouhal numbers. It is shown that both the drag and lift forces acting on the

cylinders are slightly different between the various L/D values, and the fluctuating forces peak at $L/D = 4.14$. The lift force of downstream cylinders reaches its maximum at around $\alpha = 15^\circ$. Furthermore, the flow around circular-section-cylinder arrays is also discussed in comparison with that of square cylinders.

Ivette Rodr'iguez [7][2014] It is well known that the flow past a circular cylinder at critical Reynolds number combines flow separation, turbulence transition, reattachment of the flow and further turbulent separation of the boundary layer. In the critical regime, the transition to turbulence in the boundary layer causes the delaying of the separation point and, an important reduction of the drag force on the cylinder surface known as the Drag Crisis. In this paper advanced turbulence simulations at Reynolds numbers in the range of $1.4 \times 10^5 - 8.5 \times 10^5$ will be carried out by means of large-eddy simulations. Numerical simulations using unstructured grids up to 70 million of control volumes have been performed on Marenostrum Supercomputer. One of the major outcomes is shedding some light on the shear layer instabilities mechanisms and their role on the drag crisis phenomena.

III. PROBLEM FORMULATION & TURBULENCE MODELING

3.1 Statement of Problem

The flow is in Cartesian coordinate system & the flow direction is aligned with the x-direction and the y-direction is perpendicular to the flow direction. A two dimensional square cylinder with a side B is exposed to a constant free stream velocity U_0 as shown in Fig. 3.1. The fluid is assumed to be incompressible and have constant properties. The Reynolds number is defined as $Re = (U_0 B / \nu)$ and it has been carried out at Reynolds no 22400. The dimensions of the geometry are

$B = 1.5$ (width of cylinder)

$L = 22.0$ (total length of flow domain)

$L_a = 7.0$ (approach length)
 $A = 6.0$ (length of cylinder into the paper) &
 $H = 10.0$ (width of flow domain)

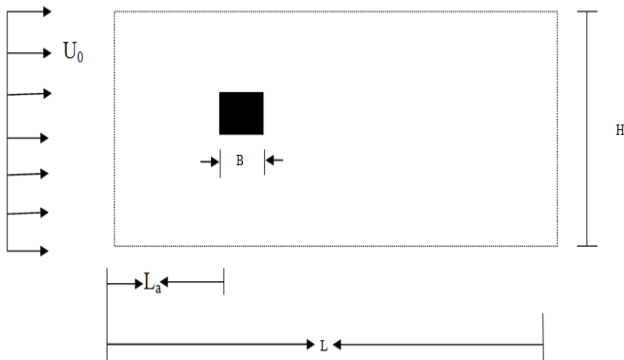


Fig 3.1 Geometrical model of flow configuration

4.1 Discretization

Discretization concerns the process of transforming continuous models and equations into discrete counterparts, means derivatives in partial differential equations are approximated by algebraic expressions which can be alternatively obtained by means of the finite-difference or the finite-element method. So the, differential equations are converted into algebraic equations involving unknown values at chosen grid points which are called as discretized equations.

4.2 Grid

Meshing is the task of partitioning a spatial domain into simple geometric elements such as triangles (in 2D) or tetrahedrons (in 3D). Grid (mesh) generation is often considered as the most important and most time consuming part of CFD simulation. The solution of a flow problem (velocity, pressure, temperature etc.) is defined at nodes inside each cell. The quality of the grid plays a direct role on the quality of the analysis, regardless of the flow solver used. The accuracy of CFD solutions is governed by number of cells in the grid. In general, the larger numbers of cells better the solution accuracy. Both the accuracy of the solution & its cost in terms of necessary computer hardware & calculation time are dependent on the fineness of the grid. Efforts are underway to develop CFD codes with a (self) adaptive meshing capability.

Ultimately such programs will automatically refine the grid in areas of rapid variation. Additionally, the solver will be more robust and efficient when using a well-constructed mesh. Basically, there exist three different types of grids.

4.2.1 Structured Grid

Each grid point (vertex, node) is uniquely identified by the indices i, j, k and the corresponding Cartesian coordinates $x_{i,j,k}, y_{i,j,k}$ and $z_{i,j,k}$, the grid cells are quadrilaterals in 2D and hexahedral in 3D. In order to resolve the boundary layers accurately, generally in 2D rectangular and in 3D prismatic or hexahedral elements are employed near solid walls. Structured grids enjoy a considerable advantage over other grid methods in that they allow the user a high degree of control. With structured grids the elements can be stretched and twisted to fit the domain because the user places control points and edges interactively, User has total freedom when positioning the mesh. So, the grid is most often flow-aligned, thereby yielding greater accuracy within the solver. Structured block flow solvers typically require the lowest amount of memory for a given mesh size and execute faster because they are optimized for the structured layout of the grid. Also, post processing of the results on a structured block grid is typically a much easier task because the logical grid planes make excellent reference points for examining the flow field and plotting the results. The major drawback of structured block grids is the time and expertise required to lay out an optimal block structure for an entire model.

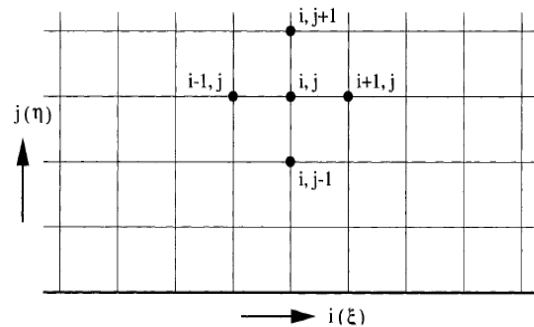


Fig (4.1) Structured body-fitted grid approach (in 2-D), i & j represents a curvilinear coordinate system

4.2.2 Unstructured Grid

Grid cells as well as grid points have no particular ordering, i.e. neighbouring cells or grid points cannot be directly identified by their indices. As these grid methods utilize an arbitrary collection of elements to fill the domain. So, the mesh is called unstructured. These types of grids typically utilize triangles in 2D and tetrahedral in 3D. The advantage of unstructured grid methods is that they are very much automated and, therefore, require little user time. The major drawback of unstructured grids is the lack of user control when laying out the mesh.

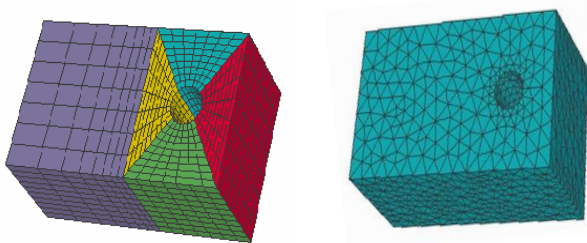


Fig (4.2) (a) Structured grid (b) unstructured grid

4.4 Discretisation Schemes

Various numerical schemes exist to do the spatial discretisation. Some of the schemes are explained here.

4.4.1 Central Schemes

These schemes are based solely on central difference formulae or on central averaging, respectively. These are denoted as central schemes. The principle is to average the conservative variables to the left and to the right in order to evaluate the flux at a side of the control volume.

$$\varphi_{f,CD} = \frac{1}{2}(\varphi_0 + \varphi_1) + \frac{1}{2}(\nabla \varphi_0 \cdot \vec{r}_0 + \nabla \varphi_1 \cdot \vec{r}_1)$$

Central-differencing schemes can produce unbounded solutions and non-physical wiggles, which can lead to stability problems for the numerical procedure. These stability problems can often be avoided if a deferred approach is used for the central-differencing scheme. In this approach, the face value is calculated as follows:

$$\varphi_f = \varphi_{f,UP} + (\varphi_{f,CD} - \varphi_{f,UP})$$

Implicit part explicit part

Where UP stands for upwind. As indicated, the upwind part is treated implicitly while the difference between the central-difference and upwind values is treated explicitly. Provided that the numerical solution converges, this approach leads to pure second-order differencing.

4.4.2 Upwind Schemes

There are more advanced spatial discretisation schemes, which are constructed by considering the physical properties of the Euler equations. Because they distinguish between upstream and downstream influences (wave propagation directions), they are termed upwind schemes. (Upwinding means that the face value ϕ_f is derived from quantities in the cell upstream, or upwind," relative to the direction of the normal velocity v_n .)

4.4.3 First-Order Upwind Scheme

When first-order accuracy is desired, quantities at cell faces are determined by assuming that the cell-center values of any field variable represent a cell-average value and hold throughout the entire cell; the face quantities are identical to the cell quantities. Thus when first-order upwinding is selected, the face value is set equal to the cell-center value of ϕ_f in the upstream cell.

4.4.4 Second-Order Upwind Scheme

When second-order accuracy is desired, quantities at cell faces are computed using a multi dimensional linear reconstruction approach. In this approach, higher-order accuracy is achieved at cell faces through a Taylor series expansion of the cell-centered solution about the cell centroid. Thus when second-order upwinding is selected, the face value ϕ_f is computed using the following expression:

$$\varphi_{f,SOU} = \varphi + \nabla \varphi \cdot \vec{r}$$

Where φ and $\nabla \varphi$ are the cell-centered value and its gradient in the upstream cell, and \vec{r} is the

displacement vector from the upstream cell centroid to the face centroid. This formulation requires the determination of the gradient $\nabla\phi$ in each cell.

IV. RESULTS AND DISCUSSION

In the present study, two dimensional numerical simulation of flow past a square cylinder has been carried out and results are compared with the experimental and numerical data available in the literature.

5.1 Time and Span-averaged Flow Field validation

The time-averaged flow field is obtained by averaging the flow field over 30-cycles. This averaging period is found to be good enough for all the velocity components. In the present study; the time-averaged and span-averaged data have been compared with the experimental results.

1] Lyn et al. (1995) and the LES results of Wang and Vanka (1996). The numerical calculations of Wang and Vanka (1996) employ a Reynolds number of 21400. Besides this the cylinder length is 20, the blockage ratio 0.05 and the inlet turbulence level is not specified and one can expect it to be negligible. The LDV experiments of Lyn et al. (1995) use a Reynolds number of 21400 and the cylinder length of 9.75. The blockage ratio was 0.07 while the inlet turbulence level was around 4%. Lyn et al. (1995) carried out the measurements at the mid- span of the cylinder and the results are available on one side of the center line ($y > 0$). In view of these differences, one cannot expect a complete match with the LDV measurements of Lyn et al. (1995) and the LES calculations of Wang and Vanka (1996) The after-body of a square cylinder, which is equal to the width of the cylinder, extends into the wake. The separated flow at the leading edges re-attaches and detaches on the top and bottom surfaces of the square cylinder and the re-attachment points on the top and bottom surfaces move back and forth (Mukhopadhyay et al.,

1992). Starting with a moderate Reynolds number the recirculation region on the top and bottom faces elongate more with increasing Reynolds number. Due to this, the recirculation bubble behind the cylinder becomes wider in the transverse direction. As a result of transverse widening of the wake. The time-averaged streamwise velocity profiles at different downstream locations ($x = 0.0, 1.0, 1.5, 2.0, 2.5$ and $x = 5$) are presented in Figures. This shows that the results due to present computation are in good agreement with their experimental counterpart. However, near the obstacle boundary (for the case of $x = 0.0$), the present computation under predicts the reverse flow. Centerline velocity is negative at the location of $x = 1.0$. The recovery of velocity is directly related to the wake-width, which in turn depends on the entrainment at the edge of the wake. The separation of flow over a bluff body causes a pressure drop across its surface and leads to a non-zero form drag. Thus a loss of momentum of the fluid is brought about in the wake. As a result, the time averaged streamwise velocity at any point in the wake is smaller than that at the free stream. This of the minimum entails attenuation velocity at the centerline. The time-averaged transverse velocity profiles, at different downstream locations ($x = 0.0, 1.0, 1.5$ and $x = 5$) are shown in figures. The transverse velocity profile at any section also indicates a measure of entrainment at that section. In any case, the transverse velocity profiles reveal good symmetry (skew symmetry) in velocities with respect to wake axis. Fig 5.8 shows the centerline recovery of the streamwise component of velocity. The recovery rate of present computation shows good agreement with Lyn et al. (1995) and Wang and Vanka (1996). However, the asymptotic value of the predicted velocity is somewhat higher and oscillates before approaching the asymptotic condition. For the sake of convenience in understanding each parameters and contours are placed one by one. Plots have been drawn for each variable for making a comparison between experimental and obtained result.

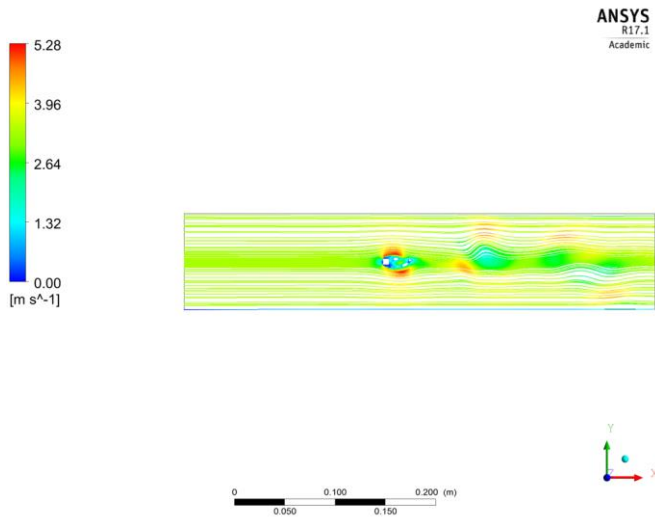


Fig.5.1 Stremline plot of time averaged flow field

The time-averaged streamline plot shown in Fig. 5.1 clearly indicates two symmetric vortices in the near wake having opposite directions of rotation (and thus satisfying conservation of angular momentum).

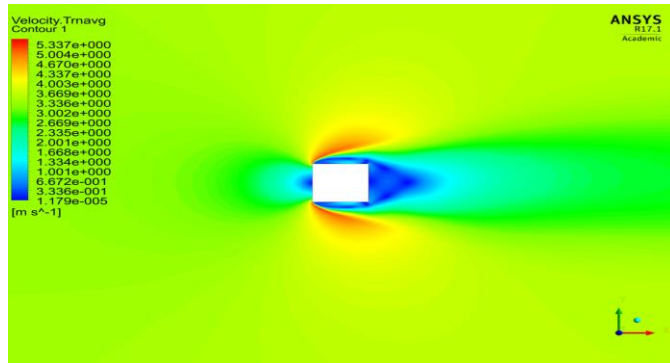


Fig.5.2 streamline plot of time average flow field

Fig.5.2 is the zoom view of stream line near the obstacle. The recirculation length is slightly larger than the width of the cylinder. In the case of a square cylinder, the separation points are fixed at the front leading edges

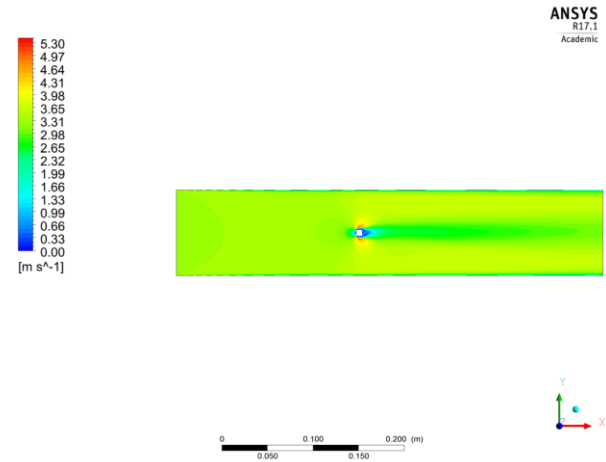


Figure 5.3 shows the streamlines at a given instant of time during the transient simulations.

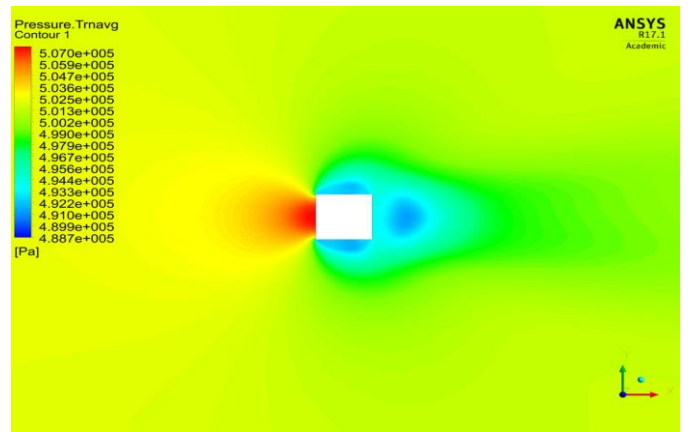


Figure 5.4 Time averaged pressure contours (averaged over 30 cycles) at Re = 22000.

This figure shows the streamlines pressure contour at a given instant of time during the transient simulations.

V. CONCLUSION

Large eddy simulation of high Reynolds number flow past a square cylinder has given the significant conclusion. This is done at 21400 Reynolds number and the important conclusions are:

- When comparing with the experimental and the large eddy simulation result with the calculated result we get the satisfactory result
- The near wake shows higher coherence, whereas in the far wake both coherent and incoherent components are of comparable magnitude.

- The vorticity and circumferential velocity in turbulent vortices are of exponential shape like those of osen vortex.
- The turbulent normal stresses and shear stresses are well predicted by the present LES computation.

VI. REFERENCES

- [1]. I. Rodr'iguez, R. Borrell, O. Lehmkuhl, C.D. P'erez-Segarra, and A. Oliva. Direct Numerical Simulation of the Flow Over a Sphere at Re 3700. *Journal of Fluid Mechanics*, 679:263–287, 2014.
- [2]. Prasenjit Dey, Ajoy Kr. Das *Engineering Science and Technology, an International Journal* 18 (2015) 758e768
- [3]. A. Rusdin *International Journal of Automotive and Mechanical Engineering* ISSN: 2229-8649 (Print); ISSN: 2180-1606 (Online); Volume 14, Issue 1 pp. 3938-3953 March 2017
- [4]. Xiaowang Sun, C. K. Chan, Bowen Mei & Zuojin Zhu (2016) LES of convective heat transfer and incompressible fluid flow past a square cylinder, *Numerical Heat Transfer, Part A: Applications*, 69:10, 1106-1124
- [5]. Wray, T. J., and Agarwal, R. K., "A New Low Reynolds Number One Equation Turbulence Model Based on a $k-\omega$ Closure," *AIAA Journal*, Vol. 53, No. 8, 2015, pp. 2216-2227., DOI:10.2514/1.J053632.
- [6]. Lyn, D. A., Einav, S., Rodi, W., and Park, J.-H., "A Laser-Doppler Velocimetry Study of Ensemble-Averaged Characteristics of Turbulent Near Wake of a Square Cylinder," *Journal of Fluid Mechanics*, Vol. 304, 1995, pp. 285–319., DOI: 10.1017/S0022112095004435.
- [7]. Lyn, D. A., and Rodi, W., "A Flapping Shear Layer Formed by Flow Separation from the Forward Corner of a Square Cylinder," *Journal of Fluid Mechanics*, Vol. 267, 1994, pp. 353–376., DOI:10.1017/S0022112094001217.
- [8]. Murakami, S., Iizuka, S., and Ooka, R., "CFD Analysis of turbulent Flow past Square Cylinder Using Dynamic LES," *Journal of Fluids and Structures*, Vol. 13, No. 78, 1999, pp.1097–1112., DOI:10.1006/jfls.1999.0246.
- [9]. Pietro, C., Meng, W., Gianluca, L., and Parviz, M., "Numerical simulation of the flow around a circular cylinder at high Reynolds numbers," *International Journal of Heat and Fluid Flow*, Vol. 24, No. 4, 2003, pp. 463-469., DOI:10.1016/S0142-727X(03)00061-4.
- [10]. Roshko, A., "On The Aerodynamic Drag of Cylinders at High Reynolds Numbers," In *Proceedings of Seminar on Wind Loads on Structures*, Honolulu, Hawaii, October 19-24

Cite this article as :

Samiran Sandilya, Amit Kumar, "A Study on Large Eddy Simulation of High Reynolds Number Flow Past A Square Cylinder", *International Journal of Scientific Research in Science, Engineering and Technology (IJSRSET)*, Online ISSN : 2394-4099, Print ISSN : 2395-1990, Volume 6 Issue 3, pp. 332-339, May-June 2019. Available at doi : <https://doi.org/10.32628/IJSRSET196335>
Journal URL : <http://ijsrset.com/IJSRSET196335>